Available online at www.sciencedirect.com
SCIENCE DIRECT
ELSEVIER
Ultramicroscopy 106 (2006) 815–821
ultramicroscopy
www.elsevier.com/locate/ultramic

Microscale Marangoni actuation: All-optical and all-electrical methods

R.H. Farahi[a], A. Passian[a,*], S. Zahrai[b], A.L. Lereu[a,c], T.L. Ferrell[a], T. Thundat[a]

[a]*Oak Ridge National Laboratory, Bethel Valley Rd., Bldg. 4500 S, MS 6123, Oak Ridge, TN 37831, USA*
[b]*Department of Mechanics, Royal Institute of Technology, Stockholm, Sweden*
[c]*Département de physique, Université de Bourgogne, 21011 Dijon, France*

Received 3 October 2005; accepted 11 December 2005

Abstract

We present experimental results from an all-optical microfluidic platform that may be complimented by a thin film all-electrical network. Using these configurations we have studied the microfluidic convective flow systems of silicone oil, glycerol, and 1,3,5-trinitrotoluene on open surfaces through the production of surface tension gradients derived from thermal gradients. We show that sufficient localized thermal variation can be created utilizing surface plasmons and/or engaging individually addressable resistive thermal elements. Both studies manipulate fluids via Marangoni forces, each having their unique exploitable advantages. Surface plasmon excitation in metal foils are the driving engine of many physical-, chemical-, and bio-sensing applications. Incorporating, for the first time, the plasmon concept in microfluidics, our results thus demonstrate great potential for simultaneous fluid actuation and sensing.

PACS: 47.85.Np; 47.27.Te; 47.55.Dz; 73.20.Mf; 07.10.Cm

Keywords: Surface plasmons; Marangoni forces; Microfluidic

1. Introduction

A characteristic property of liquids is that, although experiencing a viscous resistance, they flow when exposed to a shear stress. Solids, on the other hand, exhibit resistance to shear. Moreover, a liquid tends to form spherical drops in order to achieve the smallest surface/volume ratio, that is, it attempts to reach its lowest energy configuration. The surface energy is given by $h = \gamma - T\,\mathrm{d}\gamma/\mathrm{d}T$, where γ ($\mathrm{J\,m^2}$) is the free surface energy. In general, surface energy declines with an increase in temperature due to thermal expansion. If a droplet experiences a temperature gradient ΔT along its surface where the shear stress $\propto \Delta T$, it attempts to minimize its surface energy by moving in the direction of the gradient away from the higher temperature. This flow in the droplet was correctly interpreted by Marangoni [1] and since has been studied by others [2–7]. In the case of liquids, one often uses the term surface tension (force/unit length) instead of surface energy (energy/unit area), that is, the energy associated with the surface modes stored in the surface region. The shape of a liquid droplet, if placed on a solid surface, depends on the surface tension of 1) the open surfaces of the liquid (σ_{L}), 2) the metal surface (σ_{M}), and 3) the metal-liquid (σ_{ML}) interface, with

$$\sigma_{\mathrm{M}} = \sigma_{\mathrm{ML}} + \sigma_{\mathrm{L}} \cos\theta \quad (0 \leqslant \theta < \pi). \tag{1}$$

Using the concept of contact angle θ_{c} and neglecting the small vertical component of the surface tension, a horizontal force balance gives Eq. (1). The wetting properties of a liquid-metal pair can be determined from the observation that if $\theta_{\mathrm{c}} < 90^{\circ}$ (θ_{c} sharp), then the liquid wets the surface. Liquids with small σ_{L} readily wet most solids ($\theta_{\mathrm{c}} \approx 0$ or $\ll 90^{\circ}$), while large σ_{L} have $\theta_{\mathrm{c}} \neq 0$ [8]. Microfluidics have stimulated interest in a variety of applications where the management of microliter and nanoliter amounts of fluids can lead to fast, inexpensive and miniaturized processes, such as ''laboratories on a chip'' (lab-on-a-chip). One classification of small volume systems is an open-surface configuration that allows immediate access to the fluids under study. Marangoni

*Corresponding author. Tel.: +1 865 574 6219; fax: +1 865 574 6210.
E-mail address: passianan@ornl.gov (A. Passian).

0304-3991/$ - see front matter © 2006 Elsevier B.V. All rights reserved.
doi:10.1016/j.ultramic.2005.12.018

flow control can be practical if the localized placement of the surface tension gradient can be produced and regulated on demand, and the local environment can be kept lower than the vaporization point of the fluids. Thermal gradients may be created from several sources, thereby offering a flexible solution. We present two distinct sources of thermally derived surface tension gradients: surface plasmons (SP) and resistive heating.

We begin our presentation by discussing in Section 2 an all-optical microfluidic manipulation of silicone oil (SO) and glycerol (Gl). Optical excitation of SPs, in a thin metal film and its subsequent decay into thermal energy produce heat on the surface. By controlling the intensity and placement of thermal gradients on the surface through the control of the optical excitation, the basic microfluidic operations of transport, merge, subdivide, separate, sort and remove (desorb) are accomplished. Furthermore, SP coupling efficiency is highly sensitive to surface conditions, offering integrated sensing capabilities. In Section 3 we present microfluidic manipulation of SO and 1,3,5-trinitrotoluene (TNT) by Marangoni convective forces produced with a series of individually addressable thin-film metal resistive heater elements that dissipate power, when current is passed through them, due to the finite conductivity of the metal. The two configurations are delineated by the method in which the heat sources are produced, nevertheless the resulting convective flows are of the same origin. Concluding remarks are given in Section 4.

2. All-optical experiment and discussion

The experimental setup for a Marangoni system via SPs combines an open surface for microfluidic manipulation and an apparatus to excite SPs on a thin metal film on the surface platform, illustrated in Fig. 1. For our purposes, the optical excitation of SPs is best accomplished in the Kretschmann configuration [9], where a dielectric medium is required to increase the momentum of the electromagnetic wave so that the incident photons may excite SPs in the metal film. The configuration is a quartz prism or a quartz half-cylinder, where the metal film resides on a flat side. The incident beam with a wavelength of 514 nm from an Ar^+ laser is optically conditioned with a rotating polarizer, collimating system, and rotating mirror so that a 100 μm diameter collimated p-polarized incident beam impinges the thin metal foil at the SP angle (θ_{sp}), shown in Fig. 2. The incident angle for optimum optical coupling, is tuned to $\theta_{sp} = 52^\circ$ for the parameters of our experiment. A 34 nm smooth gold (Au) film is deposited by electron gun physical vapor deposition (PVD) at 10^{-6} Torr at a rate of 20 Å/s. The most favorable thickness of the film depends on the dielectric function of the material at the operating wavelength. The excited SPs eventually decay into optical, thermal, and acoustical energy [10,11]. It is the non-radiative decay of SPs that produces the ΔT, which may be utilized for surface-tension-driven flows of fluids on a surface [12]. One or more collimated beams of incident

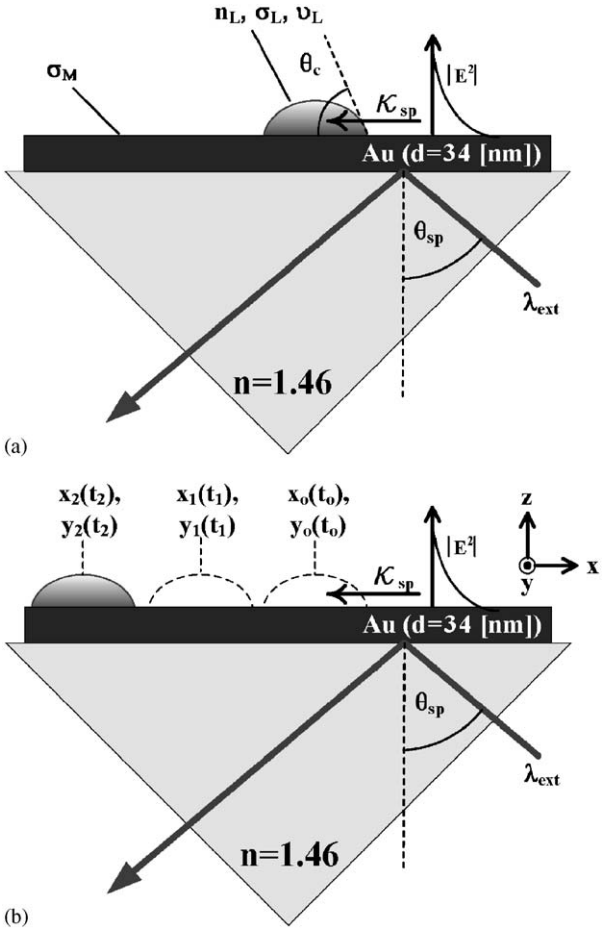

Fig. 1. Schematic of the Kretschmann configuration, including the droplets, with an incident beam λ_{ext} impinging the prism at angle θ_{sp}. Droplets (index of refraction n, surface tension σ, dynamic viscosity v, contact angle θ_c) are disposed on the surface of the gold where a temperature gradient prevails due to the decay of surface plasmons propagating in the κ_{sp} direction. The exponentially decaying field $|E^2|$ of SPs is shown for the open surface. In (a), the droplet is initially exposed to an SP excitation region at a position and time, $(x_0(t_0), y_0(t_0))$. In (b), the droplet is shown translating in the xy plane to new positions at $(x_i(t_i), y_i(t_i))$, $i = 1, 2, \ldots$.

light of various wavelengths, intensity, and locations may be placed to create localized variations in surface tension. A viewing system equipped with a CCD camera, microscope column, and a recording device was used to capture the microfluidic activity on the surface.

Manipulation of SO and Gl droplets were studied on the SP platform described in Figs. 1 and 2. For our purposes the droplet liquid and optical properties of most importance are the index of refraction (n), surface tension (σ), dynamic viscosity (v), and contact angle (θ_c). Droplets as small as 30 μm in diameter were deposited on the surface, shown in Fig. 3. The incident angle and polarization of the 514 nm laser light was tuned for maximum coupling efficiency (minimum reflected light) at the Au-air interface in the absence of the liquid. The boundary of the SP excitation region may be observed by the scattered light (bright spot) on the surface shown in Fig. 4. The calibrated

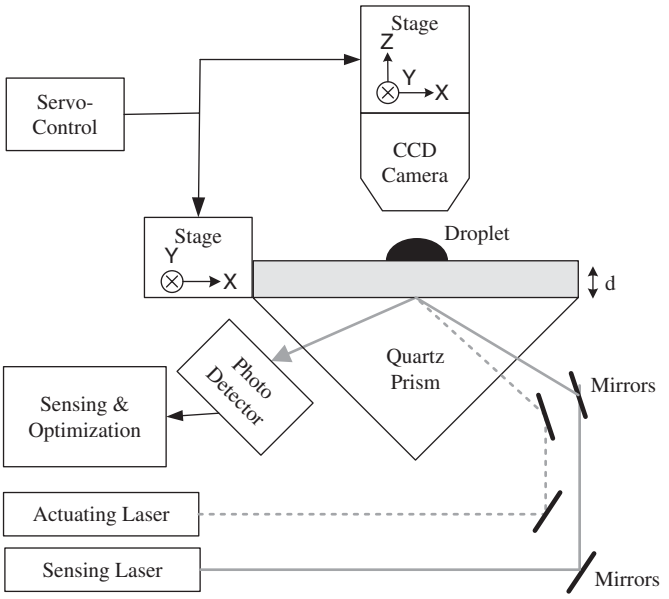

Fig. 2. Schematic representation of the experimental arrangement for surface plasmon assisted Marangoni studies, including the proposed sensing utility.

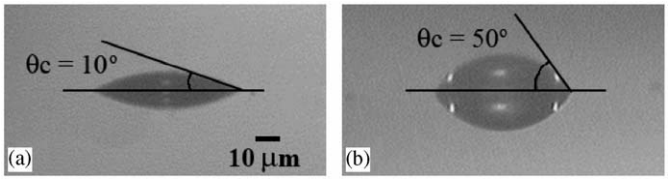

Fig. 3. Side view of 50 μm diameter droplets and their mirror images on a thin Au film. (a) Silicone oil, $n = 1.405$, $\sigma = 0.021\,\mathrm{N/m}$, $v = 0.095\,\mathrm{Pa.s}$, $\theta_c = 10^\circ$. (b) Glycerol, $n = 1.451$, $\sigma = 0.063\,\mathrm{N/m}$, $v = 1.485\,\mathrm{Pa.s}$, $\theta_c = 50^\circ$.

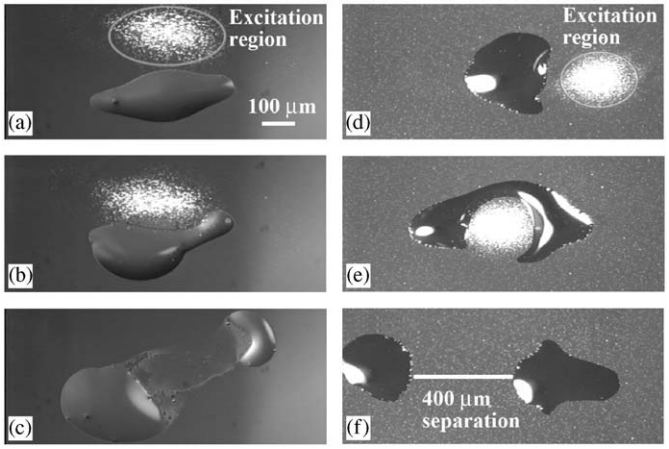

Fig. 4. Demonstration of splitting and transporting fluids by surface plasmon decay. The incident beam, generating the excitation region, a bright spot demarcated in (a) and (d), facilitates the droplet actuation.

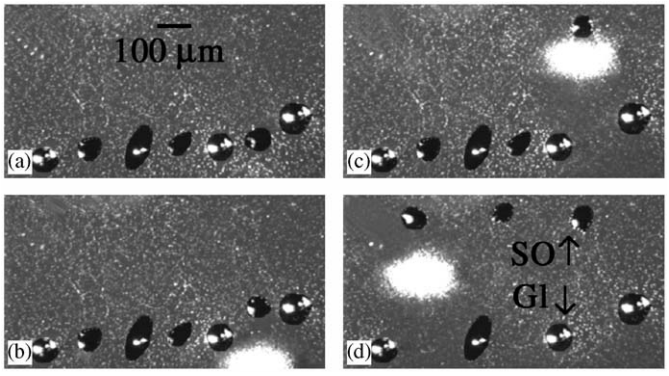

Fig. 5. Demonstration of sorting SO and Gl liquids by surface plasmons. Since the power level (45 mW) is high enough to move SO, but not sufficient for Gl, the two types of droplets may be discriminated.

power level of the laser was adjusted to provide a sufficient ΔT that will induce a convective flow of the SO droplet in Figs. 4(a)–(c) and the Gl droplet in Figs. 4(d)–(f). The minimum laser power requirement to actuate SO was 45 mW while that of Gl was 72 mW. This observation is consistent with the higher σ, v, and θ_c of the Gl. As the excitation region approaches the SO and Gl, the established ΔT caused by the decay of SP begins to induce a convective flow in the droplets. For SO, we observed a droplet speed of 100 μm/s upon the initial influence of the excitation region. If the thermal gradient expands over an area smaller than the droplet size, then the droplet will be separated as illustrated in Fig. 4.

The differentiation and sorting of fluids by Marangoni forces is demonstrated in Fig. 5. A series of droplets of SO and Gl, less than 100 μm in diameter, were interdispersed on an Au surface, Fig. 5(a). The laser power level was tuned to the minimum required to move SO (45 mW), but not sufficient for Gl. By controlling the location of the SP excitation and therefore the ensuing thermal gradient, each droplet may be visited by the thermal gradient, however only the SO droplets will be affected, as shown in Figs. 5(b)–(d). Once the SO droplets have been identified, they are segregated to another location while the Gl droplets remain, resulting in Fig. 5(d). Similar results were observed for dodecane and dodecanethiol, not shown. Since the thiol group binds to the gold surface, only the dodecane was easily transported by a thermal gradient while the docecanethiol remained static. Not only can different types of fluids be differentiated by tailoring the threshold of the ΔT to a particular analyte, any collection of droplets, similar or dissimilar, may be separated by simply targeting only the specific droplets of interest.

The optical coupling efficiency is dependent on a number of factors, including the incident polarization, incident angle, material properties of the metallic thin film, the thickness of the film, the index of refraction directly underneath and above the film, the surface roughness of the film at both interfaces, and the wavelength of incident light. The efficiency of the optical coupling is observed by measuring the intensity of the reflected spectrum. Changes in any of these conditions, through the merging of droplets of different chemical composition to form a chemical reaction for example, may be quantified in part by

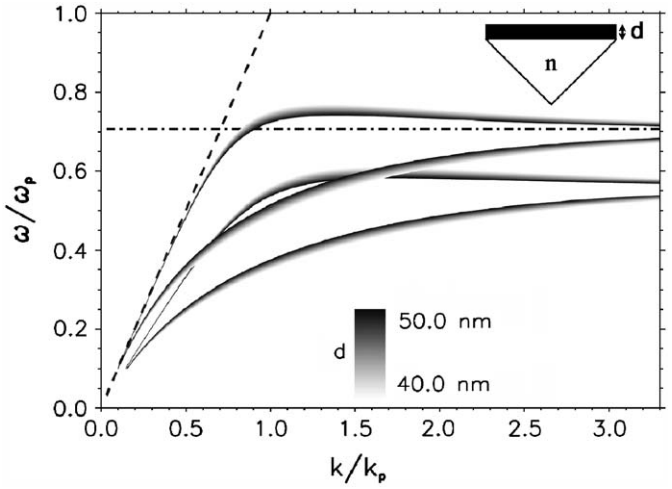

Fig. 6. The simulated red shift of the surface plasmon energies as a result of a change in the dielectric function of the bounding media. The grey scale shows the variation of foil thickness d (refer to the inset) in the range 40–50 nm. The two top branches are for a vacuum bounded slab, while the two lower curves are for a quartz ($n = 1.46$) bounded film. The dashed line represents the photon dispersion in vacuum and the dashed–dotted line marks the surface plasmon energy for the Drude model.

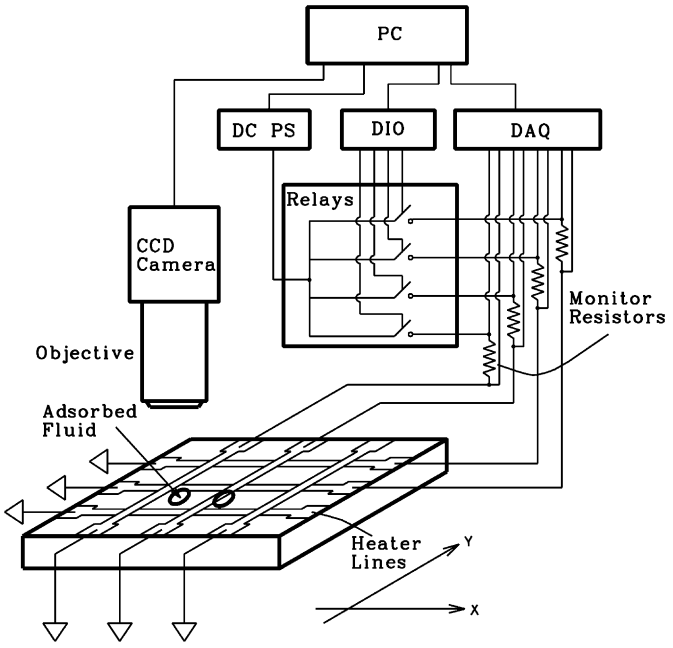

Fig. 7. Schematic representation of a two-dimensional orthogonal resistive heater network device and its control system.

monitoring the SP coupling efficiency. These parameters make tuning of the system more complex than direct optical heating [13], however we may capitalize on the sensitive nature of SP creation as a means to quantify changes in the conditions of the surface, while simultaneously actuating the fluid flow. In principle, one could use a multiple beam systems such that a single or multiple beams are used for actuation while other spectrally appropriate beams are used for sensing. As can be seen from Fig. 6, the actuation of a droplet with dielectric function of $n = 1.46$ (for example), severely red shifts the plasmon energies. However the amount of a substance to be sensed can be made small enough to allow SP sensing.

3. All-electrical experiment and discussion

Our second Marangoni-based configuration relies on the direct heating of individually addressable resistive elements as illustrated in Fig. 7. Remarkably viable resistive devices of various fashions were fabricated with an elegantly simple process. The fabrication process common to all our resistive devices is outlined in Fig. 8. Thin-film metal resistive elements are fabricated on a quartz substrate or other suitable thermally and electrically insulative material. We used 4 in diameter, 500 μm thick, polished fused quartz wafers with a thermal conductivity (1.4 W/m k) that permitted highly localized ΔT. Microscope slides with similar thermal properties also proved to be adequate substrates, but were difficult to handle in our semi-automated fabrication facility. Devices fabricated and tested with silicon wafers coated upon 2–3 μm silicon dioxide (SiO_2) or silicon nitride (Si_3N_4) were sufficiently electrically insulative, but were experimentally observed to

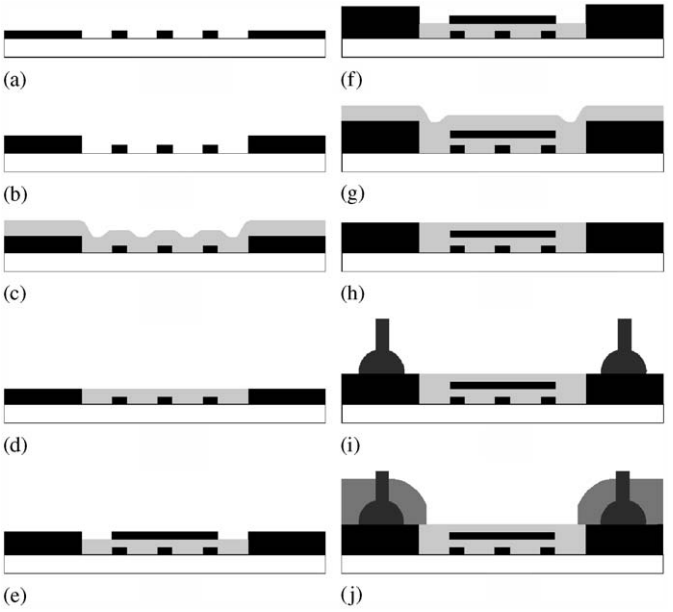

Fig. 8. Overview of the process steps for fabricating a resistive heater array device: (a) Patterned metallization of the resistive lines, connection lines, and pads; (b) additional metallization of the pads; (c) insulation layer via PECVD; (d) CMP; (e) second patterned metallization; (f) second additional metallization of the pads; (g) second PECVD; (h) CMP; (i) wafer dicing, mounting to chip carrier and wire bonding and (j) epoxy protection over the wire bonding.

be good conductors of heat, resulting in an unacceptable broad ΔT. However, wafers masked with SiO_2 or Si_3N_4 may be thinned from the backside directly underneath the heater elements to produce sharper ΔT with low power requirements. Photolithography is performed to define the resistive heater elements. The substrate is cleaned and

vapor primed in a YES oven with hexamethyldisilazane (HMDS) as an adhesion promoter. A 1.8 μm thick layer of photoresist (Shipley SPR-220 3.0) is deposited at 3500 rpm followed by a softbake for 90 s at 115 °C on a hotplate. The pattern is *i*-line exposed by a contact aligner (Karl Suss MA6), and then undergoes image reversal using a ammonia diffusion process in the oven. Afterwards, the substrate is flood exposed with the contact aligner. We found a post exposure bake for 90 s at 115 °C after image reversal improves the pattern quality. The wafer is developed (with CD-26 developer), rinsed in dionized water, and then N_2 dried. An O_2 plasma RIE for 5 s is used to descum the photoresist pattern. The photoresist pattern is metallized with a Cr adhesion layer and an Au layer using electron gun PVD at 10^{-6} Torr. Other metals such as Pt, Cr, and Al were successfully tested as well. The resistance of the heater lines ranged from 50 Ω to 1 KΩ depending on the metal and the dimensions of the resistive element.

Metal-liftoff is accomplished by dissolving the photoresist in acetone under ultrasonic agitation, establishing a metal pattern on the surface as illustrated in Fig. 8. At this point in the process, a single layer metal pattern on a substrate may be mounted and used as a device, as will be demonstrated later. However, the height of the metal pattern will eventually become an impediment to surface fluid transport. To minimize the topographical effects of the metal patterns, another series of fabrication steps are performed in Figs. 8(b)–(h). Using the same lithography techniques described above, an additional layer is deposited over the metal contact pads, illustrated in Fig. 8(b). A 500 nm thick layer of SiO_2 is deposited onto the entire wafer using a silane-based RF plasma enhanced chemical vapor deposition (PECVD) process in Fig. 8(c). The surface of the wafer is subjected to chemical mechanical polish (CMP) to smooth the surface as well as expose the protruding contact pads for wire bonding as represented in Fig. 8(d). Depending on the amount of material removal from the CMP process, the resistive elements may be buried or flush with the surface. Again, the processing may be stopped and the device may be mounted at this stage. A second level of resistive elements may be fabricated on top of the first buried layer of heater elements by repeating the same process steps of heater pattern metallization, contact pad metallization, SiO_2 PECVD, and CMP in Fig. 8(e)–(h), respectively.

Once the full-wafer fabrication steps are completed, the individual die is released by cutting the wafer with a diamond dicing saw (DAD-2H/6T dicing saw with a kerf of 50 μm). The die containing one complete resistive device is affixed to the cavity of a chip carrier with non-conductive high-temperature epoxy. The pads are electrically connected (Kulicke and Soffa wedge bonder) to the chip carrier, illustrated in Fig. 8(i). After wire-bonding the 25 μm diameter Al bond wires were coated with additional epoxy, Fig. 8(j), for protection from mechanical strain while leaving the heater array portion of the device exposed. The IC packaging of the resistive heater device offers a number of opportunities to incorporate the device in a convenient manner.

The accoutrements for activating this IC heater device are a CPU that controls a power source, a digital I/O (DIO) module, a data acquisition (DAC) system, and a viewing system. A DC power source furnishes current and voltage to the resistive elements. In this example, any thermal elements operated simultaneously would receive the same voltage and current. However, each thermal element may also be provided with independent power sources. The DIO module allows the selection of resistive elements through digitally controlled analog switches and defines the pulse-width of the electrical signals. Thus, the arrangement of power supplies and switches determines the type of electrical signals to the elements. The constructed electrical signals that would transport an adsorbed fluid may be a pulse of 20 V, 300 mA amplitude, 10 ms width, and 100 ms period with a repetition rate of 20, depending on the design of the resistive heater device. The DAC is used to monitor the power consumption through some or all of the resistive elements by monitoring the voltage through resistors in series with the elements. A wide selection of commercially available analog-to-digital boards would meet this purpose. Similar to Section 2, the viewing system is a CCD camera with an image capture board or VCR that was able to capture the fluid movements.

Depending on the application, resistive heater patterns may be designed in a number of shapes as depicted in Fig. 9. The components to a successful pattern are the geometry and pitch of the heater elements, the connection lines, which electrically unite the heater elements to the bond pads, and the bond pads which permit wire-bonding

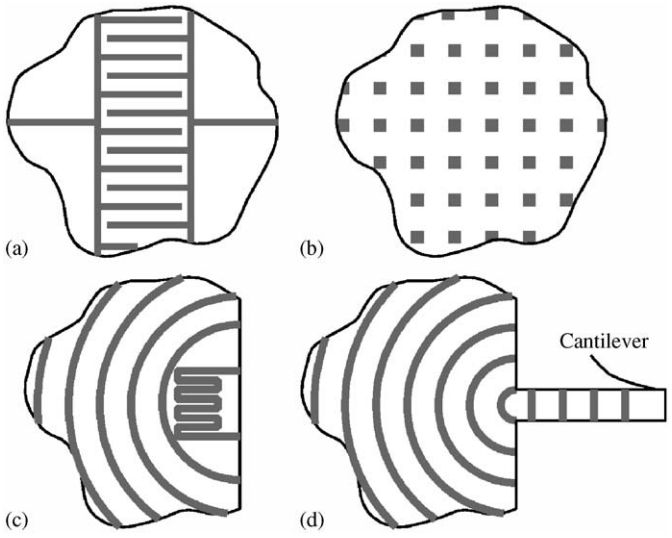

Fig. 9. Proposed heater patterns: (a) An optimized set of lines for linear transport; (b) an array of dots. The connection lines (not shown) are on multiple layers buried beneath the surface; (c) a concentric circle of heater lines with a heater pad in the center; (d) an integrated microcantilever and concentrator device.

to a chip carrier or other external structure. For example, the mask for a 96-line heater array to be mounted in a 120-pin PGA chip carrier is illustrated in Fig. 10.

Flow actuation of SO and TNT was also realized with two different geometry Au resistive heater microfluidic devices. In Figs. 11(a)–(e) and Fig. 12, the width (w), thickness (t), length (l), pitch (p), and resistance (R) are $w = 10\,\mu m$, $t = 400\,nm$, $l = 5.5\,mm$, $p = 110\,\mu m$, $R = 100\,\Omega$ and in Figs. 11(f)–(j) the dimensions are $w = 100\,\mu m$, $t = 25\,nm$, $l = 3\,mm$, $p = 200\,\mu m$, $R = 123\,\Omega$. The SO droplet in Figs. 11(a)–(e) was made by separating a much larger droplet with the activation of resistive lines. We see that the key to unlimited movements is to sufficiently transport a droplet passed the next adjacent element, so it may continue to be transported in the same direction by activating that next adjacent element. Despite the ease of flowing across the surface, there are occasions when height of the Au lines become an obstacle, shown in Fig. 11(a), (e) and (c). One solution is to add a series of processing steps to bury the heater elements in SiO_2 as described in Fig. 8, currently underway.

Surface tension gradients may induce rapid movements of liquids across a surface [14,15]. In Figs. 11(f)–(j), TNT was evaporated onto a resistive heater surface and then selectively desorbed from the right heater element. The left heater element was then pulsed at 37 V for 10 ms, causing

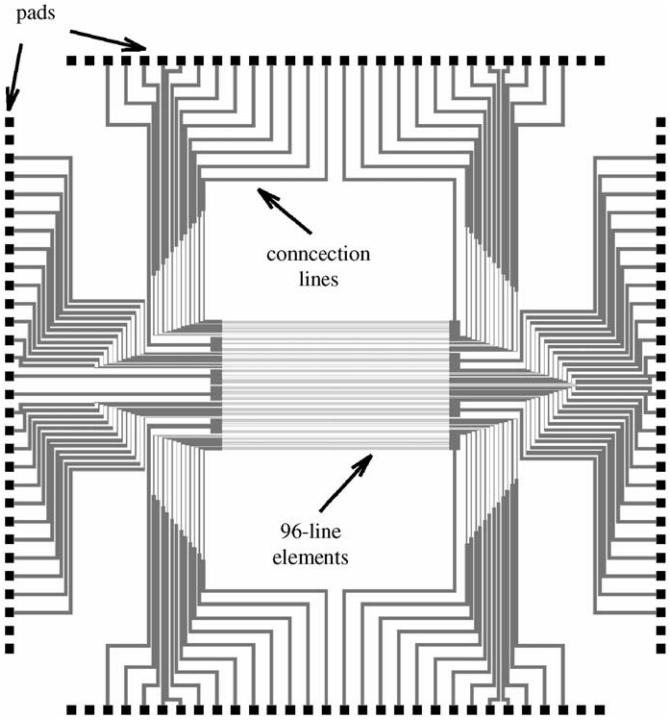

Fig. 10. A mask for a 96-line heater array with 10 μm wide lines at a 30 μm pitch. The density of the lines do not allow visual differentiation. The resistive elements (light gray) are connected to the pads (black) with intermediate connection lines (gray) that are wider and has much less resistance compared to the resistive elements. To maintain the total equivalent resistance of the lines, the meandering connection lines have exactly the same length.

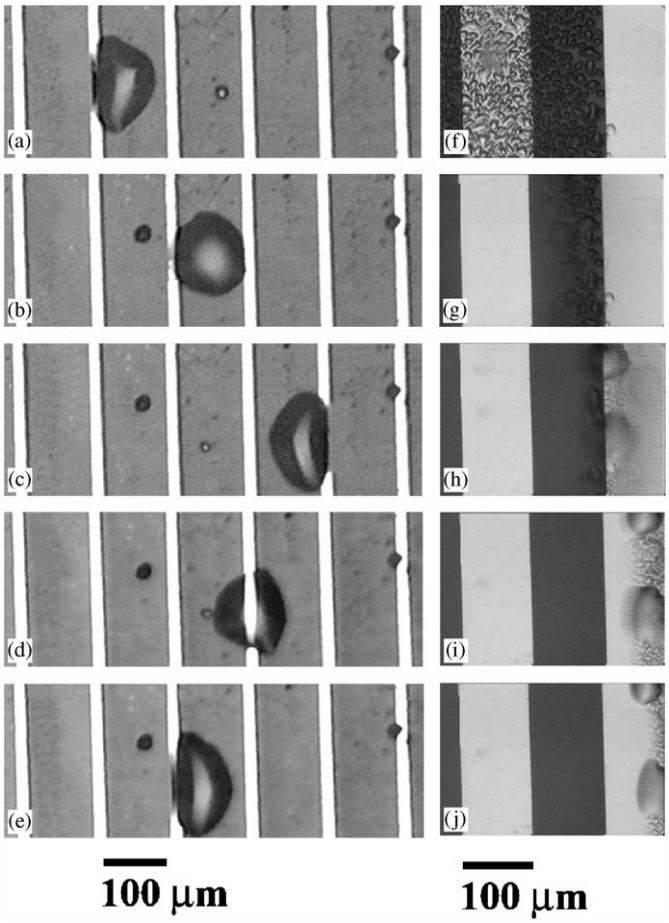

Fig. 11. Microfluidic actuation by thin-film resistive heater elements on quartz. 1D SO manipulation in (a)–(e). Fast transport of TNT in (f)–(j).

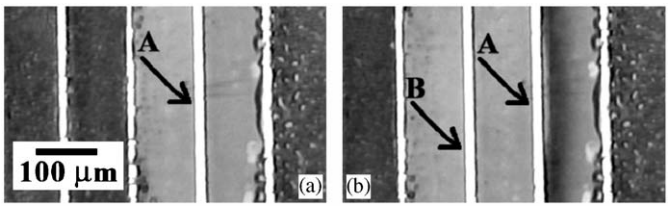

Fig. 12. Transport of evaporated TNT on a heater array surface. The resistive thin-film gold element B is actuated to cause the TNT to be transported to the right of element A.

the TNT to the right of the activated element to undergo coalescence due to the finite temperature resolution and laterally move at speeds of 1 mm/s. To minimize outright desorption directly over the heater elements, another device of 10 μm-wide heater elements was tested with adsorbed TNT, shown in Fig. 12. A pulse of 25 V for 20 ms was applied to element A in Fig. 12(a), producing a surface temperature increase that eventually evaporated most of the TNT (the vaporization point of TNT is 85 °C). However, when element B in Fig. 12(b) was pulsed, the small amount of remaining TNT to the right of element B had transported to the right and stopped just right of

element A. This type of device will be useful as a preconcentrator of trace amounts of TNT or other explosives in conjuction with a micro-sensor [16].

4. Conclusion

Microfluidic manipulation of various liquids by Marangoni forces have been conducted by two distinct heat sources, SP decay and metal thin film resistive heaters. Silicone oil, glycerol, and trinitrotoluene were used as examples to demonstrate this promising field of study. By using SP as the catalyst for convection flows, the very nature of SP excitation makes the device a very sensitive sensor of its own microfluidic manipulation. Unlike other approaches which merely control fluid transport, the use of SP provides an inherently integrated sensor as part of the microfluidic system. Resistive heaters have the advantage of being compact, simple to fabricate, free of moving parts, and easily integratable into a portable device. By spatially controlling molecules adsorbed onto a surface, these devices permit micro-scale studies of chemistry, biology, and physics. For example, fundamental studies in surface tension and interface phenomena can be explored with the operations of transport, merge, subdivide, separate, sort, remove, and capture. These approaches allow microchemical analysis of complex fluids. Analytes, cells, proteins, and DNA may be transported, separated, sorted, and merged. Parallel biological assays may be performed with small sample sizes. Micro-scale reactions may be executed by merging individual reactants in an ordered sequence. These lab-on-a-chip technologies offer a platform for disposable, fast, and inexpensive experiments. Both approaches have the potential of yielding valuable information in microfluidics research.

Acknowledgements

This research was funded in part by the Federal Aviation Administration (FAA) and the Department of Energy-Basic Energy Sciences (DOE-BES). Oak Ridge National Laboratory is operated and managed by UT-Battelle, LLC for the U.S. Department of Energy under contract number DE-AC05-00OR22725.

References

[1] C.G.M. Marangoni, Ann. Phys. Chem. (Poggendorf) 143 (1871) 337.
[2] L.E. Scriven, C.V. Sternling, Nature 187 (1960) 186.
[3] J. Thomson, Philos. Mag. Ser. 4 (10) (1855) 330.
[4] P.G. de Gennes, Rev. Mod. Phys. 57 (1985) 827.
[5] F. Brochard, Langmuir 5 (1989) 432.
[6] P. Dell'Aversana, G.P. Neitzel, Phys. Today 51 (1) (1998) 38.
[7] R. Monti, R. Savino, G. Alterio, Acta Astronaut. 51 (2002) 789.
[8] N.H. March, M.P. Tosi, Liquid State Physics, World Scientific Publishing, Singapore, 2002.
[9] E. Kretschmann, Z. Physik 241 (1971) 313.
[10] R.H. Ritchie, Phys. Rev. 106 (1957) 874.
[11] H. Raether, Surface plasmons on smooth and rough surfaces and on gratings, Springer Tracts in Modern Physics, Springer, Berlin, 1988.
[12] R.H. Farahi, A. Passian, T.L. Ferrell, T. Thundat, Opt. Lett. 30 (2005) 616.
[13] K.T. Kotz, K.A. Noble, G.W. Faris, Appl. Phys. Lett. 85 (2004) 2658.
[14] R.H. Farahi, A. Passian, T.L. Ferrell, T. Thundat, Appl. Phys. Lett. 85 (2004) 4237.
[15] S. Daniels, M.K. Chaudhury, J.C. Chen, Science 291 (2001) 633.
[16] L. Pinnaduwage, T. Thundat, J.E. Hawk, D.L. Hedden, P.F. Britt, E.J. Houser, S. Stepnowski, R.A. McGill, D. Bubb, Sensors Actuators B 99 (2003) 223.